JACS
JOURNAL OF THE AMERICAN CHEMICAL SOCIETY
Article
pubs.acs.org/JACS

Post-synthetic Structural Processing in a Metal–Organic Framework Material as a Mechanism for Exceptional CO_2/N_2 Selectivity

Witold M. Bloch,[†] Ravichandar Babarao,[‡] Matthew R. Hill,[‡] Christian J. Doonan,*[,†] and Christopher J. Sumby*[,†]

[†]School of Chemistry and Physics, The University of Adelaide, Adelaide, South Australia 5005, Australia
[‡]CSIRO Materials Science and Engineering, Private Bag 33, Clayton South MDC, Victoria 3169, Australia

Supporting Information

ABSTRACT: Here we report the synthesis and ceramic-like processing of a new metal–organic framework (MOF) material, [Cu(**bcppm**)H_2O], that shows exceptionally selective separation for CO_2 over N_2 (ideal adsorbed solution theory, S_{ads} = 590). [Cu(**bcppm**)H_2O]·*x*S was synthesized in 82% yield by reaction of $Cu(NO_3)_2·2.5H_2O$ with the link bis(4-(4-carboxyphenyl)-1*H*-pyrazolyl)methane (**H_2bcppm**) and shown to have a two-dimensional 4^4-connected structure with an eclipsed arrangement of the layers. Activation of [Cu(**bcppm**)H_2O] generates a pore-constricted version of the material through concomitant trellis-type pore narrowing (*b*-axis expansion and *c*-axis contraction) and a 2D-to-3D transformation (*a*-axis contraction) to give the adsorbing form, [Cu(**bcppm**)H_2O]-*ac*. The pore contraction process and 2D-to-3D transformation were probed by single-crystal and powder X-ray diffraction experiments. The 3D network and shorter hydrogen-bonding contacts do not allow [Cu(**bcppm**)H_2O]-*ac* to expand under gas loading across the pressure ranges examined or following re-solvation. This exceptional separation performance is associated with a moderate adsorption enthalpy and therefore an expected low energy cost for regeneration.

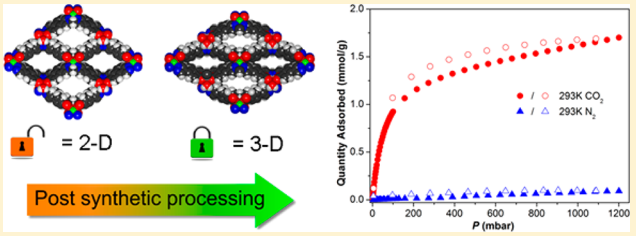

INTRODUCTION

Metal–organic frameworks (MOFs) are a burgeoning class of crystalline materials that have shown excellent potential for on-board gas storage,[1] molecular separations,[2,3] and catalysis.[4] The widespread interest in developing MOFs for these applications arises from their robust permanent porosity, high surface areas, and modular synthesis.[5] Notably, MOFs can be readily synthesized from a large range of structurally diverse organic links and metal clusters, which facilitates careful and systematic tailoring of their pore architectures and chemistry.[5] According to their framework properties upon guest removal, Kitagawa has classified MOFs as first, second, and third generation.[6] Second-generation materials have rigid, permanently porous structures that are not altered upon the removal or introduction of guest molecules; in contrast, third-generation materials exhibit a degree of flexibility or dynamic behavior that allows them to tailor their pore structures in accordance with the type of guest molecule.[7−10] Several types of behaviors are possible for dynamic MOFs, including solid-state expansion/contraction (swelling or "breathing" processes),[6,11] increases in framework connectivity (e.g., two-dimensional to three-dimensional),[6,9] and reversible and non-reversible crystal-to-crystal transformations.[6,11]

An increasingly topical area in which MOFs have shown excellent potential is selective capture of CO_2.[3] Several strategies have been used to enhance the gas separation performance of MOFs, including generation of exposed metal sites within the framework, either as part of the metal node[12] or appended to the framework via post-synthetic metalation,[13] and functionalization of the pores with Lewis basic sites.[14,15] Although these approaches have led to materials with promising performance characteristics, the underlying separation mechanism relies on increasing the affinity of the material for CO_2. Accordingly, these processes are commonly associated with higher enthalpies of adsorption for CO_2.[3d,15] A significant drawback of such strategies is that the enthalpy of adsorption of CO_2 is directly proportional to the energy cost for regeneration of the material subsequent to saturation.[16] For example, MOFs with pores functionalized by alkylamines show enthalpies of adsorption ($-Q_{st}$ values) as high as −96 kJ/mol and typically require temperatures in excess of 100 °C to fully regenerate.[3d,15,16]

Alternatively, CO_2 and N_2 can be separated by virtue of their different kinetic diameters (3.30 and 3.64 Å, respectively). Kinetic separations are not intrinsically associated with a large ΔH and therefore offer a lower energy penalty for regeneration of the adsorbent. To effectively separate adsorbates on the basis of size, precise control of the limiting pore diameter is necessary.[17,18] In this context, extended metal–organic materials with rigid but systematically tuned pore architectures have been utilized to achieve remarkable selectivities for CO_2 and N_2 separations.[17] Another approach to carefully tune the pore dimensions of MOFs is to utilize third-generation materials that have dynamic or flexible structures, as this provides an opportunity to closely tailor the required pore diameters.[10] In examples of such

Received: March 31, 2013
Published: June 12, 2013

   dx.doi.org/10.1021/ja4032049 | J. Am. Chem. Soc. 2013, 135, 10441−10448

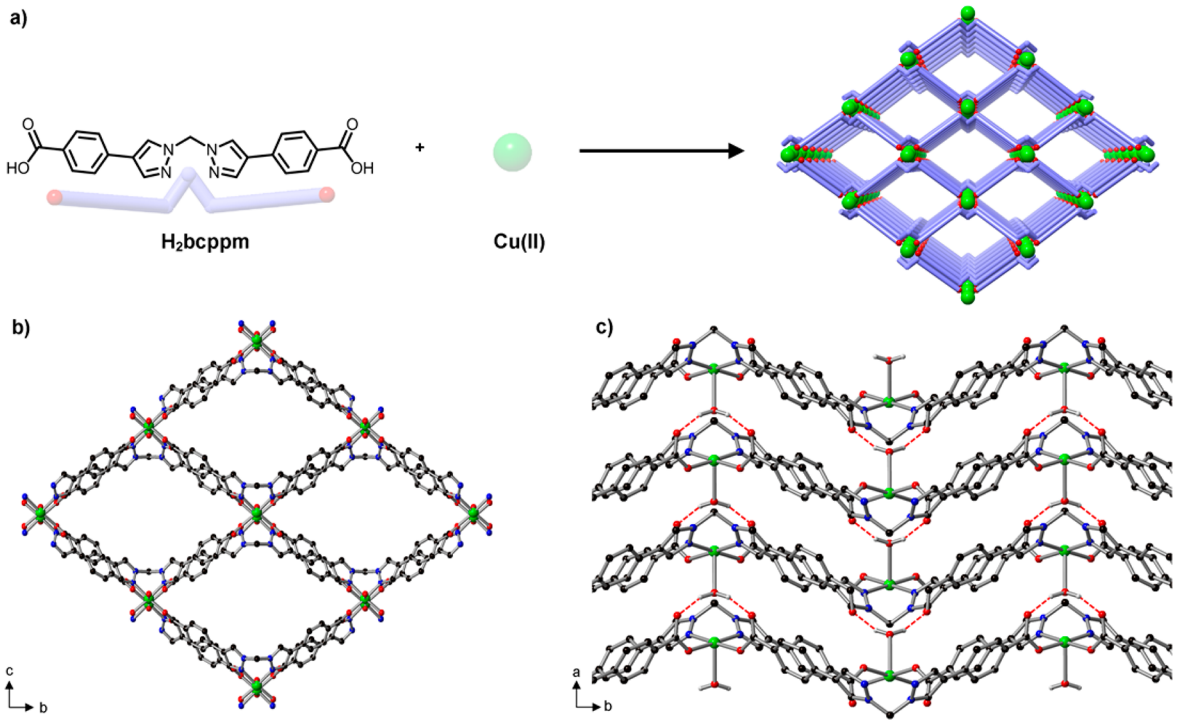

Figure 1. (a) Schematic representation of the synthesis of [Cu(**bcppm**)H_2O]·*x*S showing a simplified representation of the structure. (b) View of the pores of [Cu(**bcppm**)H_2O]·*x*S along the *a*-axis, and (c) view along the *c*-axis.

materials, only certain gases can enter the pores of a material but, once inside, induce a selective pore expansion or "gate opening".[7] A potential downside of this "gate-opening" process in gas separations is that, once "opened", these materials may act as adsorbents for all components of the gas mixture.

In this article we present the synthesis and characterization of a novel MOF material, [Cu(**bcppm**)H_2O], that subsequent to ceramic-like structural processing affords a material displaying exceptional values for CO_2/N_2 selectivity based on ideal adsorbed solution theory (IAST) calculations. As-synthesized [Cu(**bcppm**)H_2O] is a flexible 2D framework with an eclipsed 4^4 net (Figure 1), yet activation generates a material with a rigid structure and pore sizes tuned for kinetic CO_2/N_2 separations. Many examples of 2D MOFs composed of a 4^4 net are known; however, such materials are notorious for loss of crystallinity upon desolvation[9] or interlayer sliding[10] due to weak interactions between layers. Here, removal of guest molecules from the pores of [Cu(**bcppm**)H_2O] by heating results in a pore constriction, while maintaining the eclipsed arrangement of the 2D layers, and ultimately a 2D-to-3D transformation at higher temperatures. These structural changes were monitored by single-crystal and powder X-ray diffraction experiments, as well as gas adsorption measurements. Combined, these structural changes result in constriction of the limiting pore diameter to around 3.6 Å, well within the range that is suitable for kinetic CO_2/N_2 separations.[20]

EXPERIMENTAL SECTION

General Information. Elemental analyses were performed by the Campbell Microanalytical Laboratory at the University of Otago (North Dunedin, New Zealand). Thermogravimetric analysis (TGA) was performed on a Perkin–Elmer STA-6000 instrument under a constant flow of N_2 at a temperature increase rate of 10 °C/min. Infrared spectra were recorded on a Perkin–Elmer Fourier-transform infrared (FT-IR) spectrometer on a zinc–selenide crystal. NMR spectra were recorded on a Varian Gemini 300 or 600 MHz spectrometer at 23 °C using a 5 mm probe. Unless otherwise stated, all chemicals were obtained from commercial sources and used as received. The compounds di(1*H*-pyrazol-1-yl)methane (**2**)[21] and bis(4-iodo-1*H*-pyrazol-1-yl)methane (**3**)[21] were prepared by reported procedures.

Synthesis of Bis(4-(4-carboxyphenyl)-1*H*-pyrazolyl)methane (H_2bcppm). Bis(4-iodo-1*H*-pyrazol-1-yl)methane (1.01 g, 2.53 mmol), 4-carboxyphenylboronic acid (1.26 g, 7.60 mmol), and an aqueous solution of K_2CO_3 (5.00 g, 30 mL of distilled water) were combined in dimethylformamide (DMF, 135 mL). After the mixture was degassed with Ar for 30 min, $Pd(PPh_3)_4$ (0.442 g, 0.38 mmol, 0.15 equiv) was added. The resulting mixture was further degassed for 30 min and then heated at 90 °C for 20 h. Once the mixture cooled to room temperature, distilled water (200 mL) was added and the reaction mixture filtered. The resulting solution was washed with dichloromethane (5 × 50 mL) and acidified with 20% HNO_3 (pH 3) to afford a precipitate which was isolated under reduced pressure. The solid was washed with distilled water and ethanol and dried at 130 °C to give a white solid of **H_2bcppm** (0.68 g, 69%) Mp: 350–352 °C (dec.). Elemental analysis: found C 64.2, H 4.0, N 14.4; $C_{21}H_{16}N_4O_4·0.25H_2O$ requires C 64.2, H 4.2, N 14.3%. IR ν_{max} (neat, cm^{-1}): 1701 (C═O), 1613 (C═N), 1568 (C═C), 1508 (C═C). ^{1}H NMR (300 MHz/DMSO): δ 6.47 (s, 2H, CH_2), 7.72 (d, 4H, H2′/H6′), 7.91 (d, 4H, H3′/H5′), 8.09 (s, 2H, H3 or H5), 8.56 (s, 2H, H3 or H5), 12.8 (s, br, 2H, CO_2H). ^{13}C NMR (150 MHz/DMSO): δ 65.0, 122.0, 125.0, 128.4, 128.6, 130.0, 136.3, 138.3, 167.0.

Synthesis of [Cu(bcppm)H_2O]·*x*S (*S* = solvate). In a screw-cap vial, $Cu(NO_3)_2·2.5H_2O$ (36.3 mg, 0.16 mmol) and **H_2bcppm** (41.5 mg, 0.11 mmol) were dissolved in a mixture of DMF (2 mL), distilled water (0.5 mL), ethanol (0.5 mL), and 2 drops of 70% HNO_3. The resulting mixture was heated at 85 °C for 16 h, affording blue block-like crystals suitable for X-ray crystallography. The crystals were soaked in DMF (×3) and acetone (×8) and heated at 120 °C under high vacuum for 3 h to yield a green crystalline powder, [Cu(**bcppm**)H_2O]-*ac* (*ac* = activated) (40.8 mg, 82%, based on analysis). IR ν_{max} (neat, cm^{-1}): 3125 (w, C–H), 2800–3300 (br, OH), 1608 (m, C═O), 1581 (m, C═C), 1545 (m, C═C), 1377 (s, C–O). Elemental analysis: found C 53.80, H 3.43, N 12.23; $C_{21}H_{16}N_4O_5Cu$ requires C 53.90, H 3.45, N 11.97%.

dx.doi.org/10.1021/ja4032049 | J. Am. Chem. Soc. 2013, 135, 10441–10448

X-ray Crystallography. Single crystals were mounted in paratone-N oil on a plastic loop. X-ray diffraction data were collected with Mo Kα radiation (λ = 0.7107 Å) using an Oxford Diffraction X-calibur single-crystal X-ray diffractometer at 150(2) K. Data sets were corrected for absorption using a multi-scan method, and structures were solved by direct methods using SHELXS-97[22] and refined by full-matrix least-squares on F^2 by SHELXL-97,[23] interfaced through the program X-Seed.[24] In general, all non-hydrogen atoms were refined anisotropically and hydrogen atoms were included as invariants at geometrically estimated positions, unless specified otherwise in additional details below. Figures were produced using the program CrystalMaker.[25] Publication materials were prepared using CIFTAB.[26] CCDC 930403 and 930404 contain the supplementary crystallographic data for these structures. These data can be obtained free of charge from The Cambridge Crystallographic Data Centre via www.ccdc.cam.ac.uk/data_request/cif. X-ray data are given in Table 1.

Table 1. Crystal Data and Experimental X-ray Data for [Cu(bcppm)H_2O]·*xS* and [Cu(bcppm)H_2O]-*heated*

	[Cu(**bcppm**)H_2O]·*xS*	[Cu(**bcppm**)H_2O]-*heated*
empirical formula	$C_{21}H_{16}CuN_4O_5$	$C_{21}H_{16}CuN_4O_5$
formula weight	467.92	467.92
crystal system	orthorhombic	orthorhombic
space group	*Pnma*	*Pnma*
a (Å)	9.9995(3)	8.800(3)
b (Å)	19.2590(4)	20.734(2)
c (Å)	15.3449(5)	13.110(5)
V (Å^3)	2955.13(14)	2392.0(12)
Z	4	4
D_{calc} (Mg/m^3)	1.052	1.299
absorption coefficient (mm^{-1})	0.768	0.949
F(000)	956	956
crystal size (mm^3)	0.21 × 0.14 × 0.08	0.33 × 0.16 × 0.12
θ range for data (°)	2.65−29.24	2.79−24.99
reflections collected	14352	11882
independent reflns [R(int)]	3605	2159
completeness to θ full (%)	98.9	99.7
observed reflns [$I > 2\sigma(I)$]	2892 [0.0404]	1133 [0.0862]
data/restraints/parameters	3605/0/205	2159/2/126
GOF on F^2	1.062	1.562
R_1 [$I > 2\sigma(I)$]	0.0452	0.1937
wR_2 (all data)	0.1382	0.4948
largest diff. peak and hole (e Å^{-3})	0.587, −0.325	2.383, −0.753

Special Refinement Details for [Cu(bcppm)H_2O]·*xS*. The structure has large, solvent-accessible voids. These contain a number of diffuse electron density peaks that could not be adequately identified and refined as solvent. The SQUEEZE routine of PLATON[27] was applied to the collected data, which resulted in significant reductions in R_1 and wR_2 and an improvement in the goodness-of-fit (GOF). R_1, wR_2, and GOF: before SQUEEZE routine, 9.82%, 35.53%, and 1.53; after SQUEEZE routine, 4.52%, 13.8%, and 1.06. There is some disorder in the structure, and the aryl ring and carboxylate group were modeled over two positions.

Special Refinement Details for [Cu(bcppm)H_2O]-*heated*. The structure has large, solvent-accessible voids. These contain a number of diffuse electron density peaks. The SQUEEZE routine of PLATON[27] was applied to the collected data, which resulted in reasonable reductions in R_1 and wR_2 and an improvement in the GOF. R_1, wR_2, and GOF before SQUEEZE routine: 25.5%, 60.2%, and 1.72; after SQUEEZE routine: 19.4%, 49.5%, and 1.56. The data are of relatively poor quality due to the conditions used to generate the sample (heating in an oven at 80 °C).

Powder Diffraction. Powder X-ray diffraction data were collected on a Rigaku Hiflux Homelab system using Cu Kα radiation with an R-Axis IV++ image plate detector. Samples were mounted on plastic loops using paratone-N and data collected by scanning 90° in ϕ for 120−300 s exposures. The data were converted into xye format using the program Datasqueeze 2.2.2, Datasqueeze Software; Wayne, Pennsylvania, U.S.A., 2010. Simulated powder X-ray diffraction patterns were generated from the single-crystal data using Mercury 2.4.[28] Variable-temperature powder X-ray diffraction (VT-PXRD) was carried out at the Australian Synchrotron on the Powder Diffraction beamline. The sample was prepared in a glass capillary (0.3 mm) and exposed to X-rays with a wavelength of 0.82544 Å. For further details on the instrument setup, see www.synchrotron.org.au. Further data on the activated [Cu(**bcppm**]H_2O] were collected on a Bruker X'Pert instrument with Co Kα radiation.

Simulation Methods. Geometric pore size distributions were calculated on the basis of a Monte Carlo technique using the procedure described elsewhere.[29] The accessible void surface was determined on the basis of a probe diameter of 3.3 Å, which is equal to the kinetic diameter of CO_2, using the Atom Volumes and Surfaces tool within Materials Studio V6.0.0 from Accelrys Software Inc. To locate the preferential CO_2 adsorption site in [Cu(**bcppm**)H_2O]-*ac*, a simulated annealing method was employed using an in-house code. A universal force field was used to describe the [Cu(**bcppm**)H_2O]-*ac* framework atoms and a three-site model for the CO_2 molecule.[30] The total energy of the system was approximated as the sum of all pairwise intermolecular interactions by a Lennard-Jones potential and Coulombic interactions. In the simulated annealing method, the temperature was lowered in succession, allowing the gas molecule to reach a desirable configuration based on different moves such as rotate, translate, and re-position with preset probabilities of occurrence. This process of heating and cooling the system was repeated in several cycles to find the local minima. Forty heating cycles were performed where the maximum temperature and the final temperature were 10^5 and 100 K, respectively. The NVT ensemble process consisted of 10^7 equilibration steps followed by 10^7 production steps, with the properties calculated from the latter steps.

For predicting gas mixture selectivity, IAST was employed.[31] IAST has been widely used and tested to predict gas mixture selectivity in MOFs and zeolites, and it showed good agreement with the predicted simulation selectivity and gas mixture adsorption experiments.[17,32] In this work, dual-site and three-site Langmuir−Freundlich equations were used to fit the adsorption isotherm of pure CO_2 and N_2 gas. The fitted parameters (Supporting Information (SI) Table S3) were then used to predict the adsorption of a mixture. Adsorption selectivity was calculated by $S_{ads} = (q_1/q_2)/(p_1/p_2)$, where q_1 and q_2 are the amounts adsorbed at the partial pressures p_1 and p_2, respectively.

Gas Adsorption Measurements. Gas sorption isotherm measurements were performed on an ASAP 2020 surface area and pore size analyzer. A sample of [Cu(**bcppm**)H_2O]·*xS* was soaked and washed at least eight times with acetone during the course of 2 h to remove the non-coordinated solvent molecules. The mixture was transferred into an ASAP 2020 analysis tube, and the solvent was carefully decanted. After removal of the residual acetone by drying under an N_2 stream, the sample was activated under vacuum at 120 °C for 3 h to obtain [Cu(**bcppm**)H_2O]-*ac*. UHP-grade (99.999%) N_2 and CO_2 were used for all measurements. The temperatures were maintained at 77 (liquid nitrogen bath), 195 (acetone−dry ice bath), 273 (ice−water bath), or 293 K (room-temperature water). CO_2 enthalpy plots were obtained with the use of Van't Hoff plots derived from isotherms collected at 273 and 293 K.

RESULTS AND DISCUSSION

Synthesis and Structure of [Cu(bcppm)H_2O]·*xS*. **H_2bcppm** was synthesized in one step (69% yield) from commercially available 4-carboxyphenylboronic acid and readily synthesized bis(4-iodo-1*H*-pyrazol-1-yl)methane.[21] Reaction of **H_2bcppm** with $Cu(NO_3)_2$ under solvothermal conditions gave [Cu(**bcppm**)H_2O]·*xS* after 16 h. It was essential to include 0.25 mL of H_2O per 1 mL of DMF in the solvent mixture to obtain the desired material. Although [Cu(**bcppm**)H_2O]·*xS* could be

dx.doi.org/10.1021/ja4032049 | J. Am. Chem. Soc. 2013, 135, 10441−10448

prepared in DMF with added water, addition of EtOH and HNO_3 (70%, 2 drops) to the solvothermal reaction resulted in the formation of large and regular block-shaped blue crystals suitable for single-crystal X-ray crystallography. X-ray crystallography revealed a 2D structure with a 4^4 net (Figure 1a) composed of chelating dipyrazolyl moieties that bridge to adjacent copper atoms via the phenyl-carboxylate groups (Figure 1b). The square-pyramidal copper(II) center is coordinated by one chelating dipyrazolylmethane unit, two monodentate carboxylate donors from two further **bcppm** moieties, and a single water molecule.

As shown in Figure 1b, the 4-connected 2D layers of [Cu(**bcppm**)H_2O]·*xS* are eclipsed and give rise to regular diamond-shaped channels that propagate along the *a*-axis. The alignment of the windows in [Cu(**bcppm**)H_2O]·*xS* is driven by strong interlayer hydrogen bonding between the hydrogen atoms of the water ligands in one layer and the carbonyl oxygen atoms from an adjacent layer (Figure 1c and Figure 2, left,

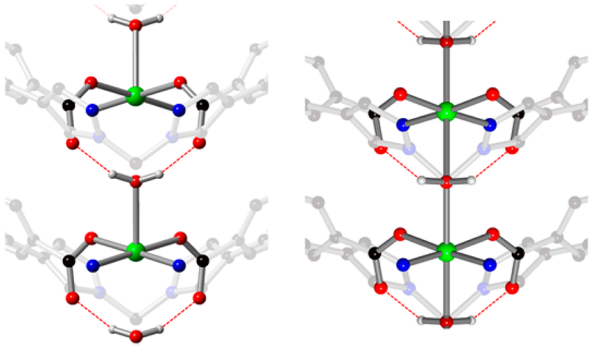

Figure 2. Enlargements of the hydrogen bonding in (left) [Cu(**bcppm**)H_2O]·*xS* (between the 2D layers) and (right) [Cu(**bcppm**)H_2O]·*heated*.

O−H···O: $d_{H\cdots O}$ = 2.00 and 2.06 Å, $D_{O-H\cdots O}$ = 2.69 and 2.71 Å, angle = 162.9 and 153.1°). The structure has solvent-accessible channels along the *a*-axis (pore diameter of ca. 6.9 Å), yet in the *b*- and *c*-axes [Cu(**bcppm**)H_2O]·*xS* is essentially close-packed (Figure 1c). PXRD on a bulk sample [Cu(**bcppm**)H_2O]·*xS* indicated that the material was phase pure (Figure 3).

Post-synthetic Processing. During activation of [Cu(**bcppm**)H_2O], a distinct color change of the crystalline material, from blue to green, was observed. The activated material, [Cu(**bcppm**)H_2O]-*ac*, was obtained by heating an acetone-solvated sample under vacuum at 120 °C for 3 h. Upon inspection of the PXRD pattern of [Cu(**bcppm**)H_2O]-*ac*, we noticed a distinct shift in the spacing of the 011 and 020 planes (refer to SI and Figure 3), indicating a structural modification had occurred. TGA of [Cu(**bcppm**)H_2O]-*ac* showed minimal weight loss and indicated that the material is thermally stable to 285 °C (Figure SI 1). [Cu(**bcppm**)H_2O]-*ac* could be re-solvated but did not recover the original unit cell dimensions. Even after [Cu(**bcppm**)H_2O]-*ac* was heated in methanol at 65 °C, the original structure could not be regenerated (Figure SI 5), indicating a permanent and irreversible transformation during the post-synthesis processing.

Despite considerable effort to obtain a structure for [Cu(bcppm)H_2O]-*ac*, the decrease in the observed crystallinity thwarted **bcppm** all approaches to characterize this particular phase by X-ray diffraction methods. Further understanding of the structural changes during post-synthetic processing that lead to [Cu(**bcppm**)H_2O]-*ac* was provided when single crystals were obtained from a sample heated to 80 °C ([Cu(**bcppm**)H_2O]-

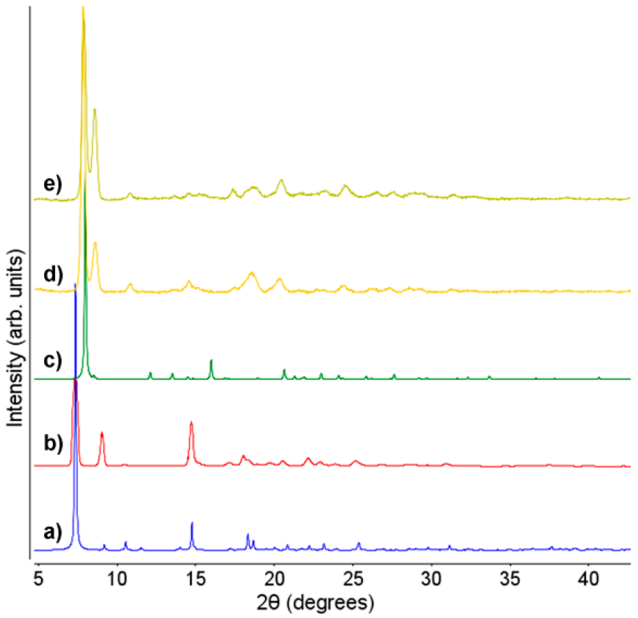

Figure 3. PXRD patterns of (a) [Cu(**bcppm**)H_2O]·*xS* (blue, simulated); (b) [Cu(**bcppm**)H_2O]·*xS* (red); (c) [Cu(**bcppm**)H_2O]-*heated* (green, simulated); (d) [Cu(**bcppm**)H_2O]-*ac* (yellow); and (e) [Cu(**bcppm**)H_2O]-*ac* exposed to 1 bar of CO_2 (khaki).

heated). This crystal structure revealed that the material has undergone a prominent trellis-like contraction, narrowing along the *c*-axis and elongating along the *b*-axis (Figure 4a versus 4b), and a 2D-to-3D transformation. 2D-to-3D transformations are commonly encountered in 2D materials as a result of changes in the coordination sphere of the metal due to desolvation, or through ligand insertion or substitution reactions.[33] In [Cu(**bcppm**)H_2O]-*heated*, the *a*-axis has been noticeably shortened from 9.9995(3) Å in the as-synthesized material to 8.800(3) Å. This occurs with a change in the coordination environment of the copper(II) center from five coordinate to a Jahn−Teller distorted octahedral six coordinate (Figure 2, right) and, as a consequence of a now bridging water ligand, to a 3D structure. This form of the structure is also reinforced by noticeably shorter hydrogen bonding between the bridging water ligand and a carboxylate in the adjacent layer (O−H···O: $d_{H\cdots O}$ = 1.73 Å, $D_{O-H\cdots O}$ = 2.59 Å, angle = 143.3°). These combined structural changes explain why the expanded material cannot be regenerated upon re-solvation and the material is "locked" in a contracted state. Calculations on an energy-minimized form of [Cu(**bcppm**)H_2O]-*heated* reveal that the material has a limiting pore diameter of 3.6 Å (pore size maximum of 4.5 Å), perfect for kinetic separation of gases like CO_2 and N_2. It is also reasonable to suggest that this behavior, along with secondary sphere effects (hydrogen bonding and loss of pore solvent), accounts for the distinct color change of this material during activation.

We further probed the post-synthetic processing of [Cu(**bcppm**)H_2O] by variable-temperature synchrotron PXRD experiments. These experiments were undertaken in sealed capillaries and were used to continuously monitor the structural changes of two solvated samples: [Cu(**bcppm**)H_2O]·*xS* and [Cu(**bcppm**)H_2O]-*acetone* (Figure 4). Depending on the boiling point of the solvates included in the framework, PXRD confirms that [Cu(**bcppm**)H_2O] undergoes the trellis-like structural change, namely elongation and contraction of the *b*- and *c*-axes, respectively; a gradual contraction is observed for the as-synthesized form, while the acetone-exchanged form displays a rapid transition. The PXRD data were indexed up to

dx.doi.org/10.1021/ja4032049 | J. Am. Chem. Soc. 2013, 135, 10441−10448

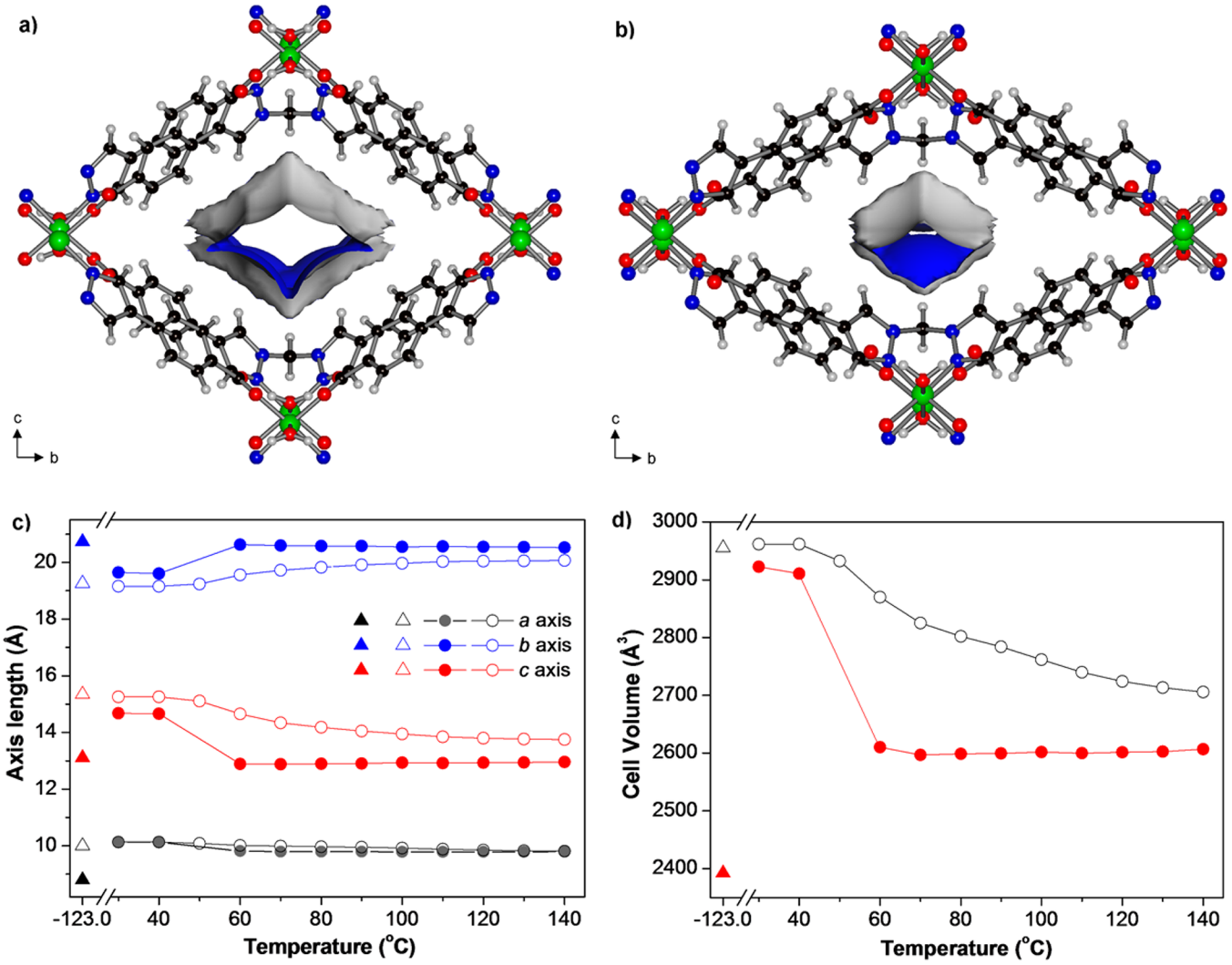

Figure 4. Representations of the crystal structures of (a) [Cu(**bcppm**)H_2O]·*xS* and (b) [Cu(**bcppm**)H_2O]-*heated* showing the solvent-accessible pore surface with a probe of diameter 3.30 Å. Color - Cu, green; C, Black; N, Blue; O, Red; H, Grey. (c) Temperature-dependent changes of the unit cell axes determined from indexing the PXRD data: open circles, [Cu(**bcppm**)H_2O]·*xS*; filled circles, [Cu(**bcppm**)H_2O]-*acetone*. Open and filled triangles represent the unit cell dimensions from the crystal structures of [Cu(**bcppm**)H_2O]·*xS* and [Cu(**bcppm**)H_2O]-*heated*, respectively. (d) Temperature-dependent changes of the unit cell volume: open black circles, [Cu(**bcppm**)H_2O]·*xS*; red circles, [Cu(**bcppm**)H_2O]-*acetone*; black triangle, cell volume from the crystal structure of [Cu(bcppm)H_2O]·*xS*; red triangle, cell volume of [Cu(**bcppm**)H_2O]-*heated*.

140 °C, as after this point the crystallinity diminished and the activated 3D form [Cu(**bcppm**)H_2O]-*ac* was obtained. At 140 °C the *a*-axis was reduced by only ~0.33 Å, indicating that the water remains coordinated to only one copper center and the material has yet to undergo the 2D-to-3D transition. This transition takes place above 140 °C under the experimental conditions (sealed capillary) and is accompanied by reductions of long-range order and a further shift of the 011 and 020 Miller planes. We note that peak broadening and a decrease in observed crystallinity are known for layered materials and result from shifts in the interlayer packing[6,9] and, in this case, the 2D-to-3D transformation. Finally, we observed that the important Miller indices (011 and 020) of the activated material closely match data simulated from the single-crystal structure of [Cu(**bcppm**)H_2O]-*heated* (Figures 3 and SI 4).

To probe the "locked" nature of [Cu(**bcppm**)H_2O]-*ac*, we investigated whether the material responds structurally to gas adsorption at pressures relevant for post-combustion CO_2 capture, i.e., whether adsorption of CO_2 gas is accompanied by an undesirable expansion of the structure. This would amount to "gate opening", thus increasing the pore diameter and essentially reducing the selectivity of this material in a mixed gas stream. Therefore, we performed PXRD experiments on [Cu(**bcppm**)H_2O]-*ac* in the presence of CO_2. Satisfyingly, no change was observed in the PXRD pattern at 1 bar of CO_2 at room temperature (Figure 3e), indicating that the material remains contracted, or in a "locked" state, and retains its constricted pore diameter upon adsorption of CO_2 gas. Furthermore, the material also displays reasonable stability to water, due to its narrow pore dimensions and relatively hydrophobic channel structure, and can be soaked in water for 24 h without appreciable loss of crystallinity.

Gas Adsorption. [Cu(**bcppm**)H_2O] was shown to be essentially non-porous to N_2 gas at 77, 273, and 293 K (Figures SI 6 and 7) but porous to CO_2 at 273 and 293 K (Figure 5a). Furthermore, we saw no appreciable uptake of CO_2 at 195 K, which confirms that the limiting pore diameters of the material are very close to the kinetic diameter of CO_2 at low temperatures (a likely explanation is that CO_2 molecules cannot enter the pores at 195 K due to large diffusional resistances, but at 273 and 293 K the additional thermal energy

dx.doi.org/10.1021/ja4032049 | J. Am. Chem. Soc. 2013, 135, 10441−10448

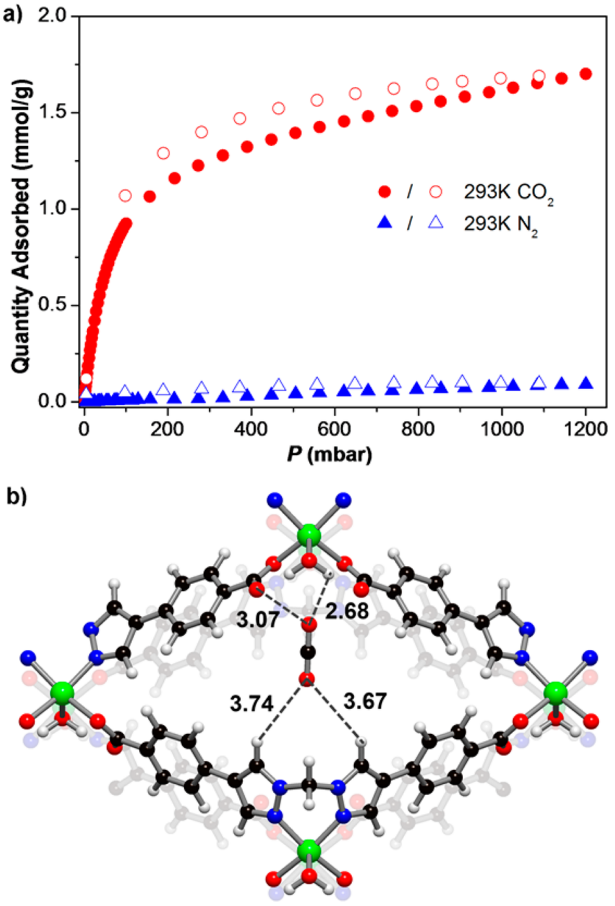

Figure 5. (a) CO_2 and N_2 isotherms at 293 K. (b) A view showing the location of CO_2 in [Cu(**bcppm**)H_2O]-*ac* identified from NVT-simulated annealing. Selected distances between the CO_2 molecule and the framework atoms are shown in angstroms.

allows the molecules to overcome these resistances).[32,34] A BET surface area was calculated using the adsorption isotherm for CO_2 at 273 K using criteria detailed elsewhere.[32] A surface area of 155 m^2/g was obtained, and this compares favorably with the geometric surface area calculated for [Cu(**bcppm**)-H_2O]-*heated* of 175 m^2/g. A pore size distribution obtained from the 273 K CO_2 isotherm (Figure SI 9) provides a limiting pore size of 3.6 Å, which matches[35] that calculated from the single-crystal structure of [Cu(**bcppm**)H_2O]-*heated*.

Figure 5a shows that the uptake of N_2 at 293 K reaches a maximum of only 0.09 mmol/g at 1200 mbar. In contrast, CO_2 gas adsorption isotherms at 273 and 293 K clearly show that the pore structure of [Cu(**bcppm**)H_2O]-*ac* is readily accessible to the smaller adsorbate at these temperatures. The total CO_2 uptakes at 293 and 273 K are 1.70 and 1.85 mmol/g, respectively (Figure SI 9). Inspection of the CO_2 isotherms (Figure 5a) shows steep uptake in the low-pressure region, with an initial calculated enthalpy of adsorption for CO_2 of −29 kJ/mol. The moderate heat of adsorption (Table 2) is consistent with an absence of strong adsorption sites and can be rationalized by a constricted pore space facilitating interactions with the pore walls. NVT-simulated annealing suggests that CO_2 weakly interacts with multiple oxygen and hydrogen atoms that line the pore walls (Figure 5b). The predicted heat of adsorption from NVT simulation is around −29.5 kJ/mol, which is in excellent agreement with the experimental value. Similar multi-point CO_2−framework interactions were recently observed in a MOF material where the pores acted as single-molecule traps.[18] The observed hysteresis in the CO_2 isotherms can be attributed to the small pore windows in the MOF. The relatively high CO_2 and marginal N_2 uptake at ambient temperature prompted us to investigate the capacity of [Cu(**bcppm**)H_2O] to selectively adsorb CO_2 over N_2. From the single-component isotherms the wt% of CO_2 (0.15 atm) and N_2 (0.85 atm) was found to be 4.64% and 0.22%, respectively. The potential for a material to perform separations from a mixed gas stream can be estimated using IAST. In terms of prediction, IAST gives the closest approximation of binary gas selective adsorption performance from single-component isotherms.[17,32] IAST calculations performed on [Cu(**bcppm**)-H_2O]-*ac* yield a selectivity for CO_2/N_2 (15/85 wt% mixture) of 590 at 293 K and 1 atm. Table 2 shows that [Cu(**bcppm**)H_2O] outperforms all but one state-of-the-art MOF and zeolite materials. This is remarkable, given that the material lacks both unsaturated metal centers and amine groups. However, we note that the total CO_2 uptake capacity of [Cu(**bcppm**)H_2O] is moderate compared to high surface area MOFs such as MOF-74. During the course of this work, SIFSIX-3-Zn, a material that also displays exceptional CO_2/N_2 selectivity, was reported. SIFSIX-3-Zn has more-regular square-shaped channels with dimensions of 3.84 Å and lined with Lewis basic groups on the SiF_6 anions that notably enhance the uptake of CO_2 into the material, giving a Q_{st} of −45 kJ mol^{-1} at low loading.

As outlined elsewhere,[16] for MOFs to be economically viable for CO_2 capture, the selectivity, capacity, and enthalpy of adsorption need to be carefully considered. This has led to the employment of various strategies to increase the affinity of a material for CO_2, including Lewis bases,[14,15] interpenetration,[3b] and unsaturated metal sites.[12,13] Lewis bases are known to imbue materials with exceptional selectivity; however, this is commonly associated with a high enthalpy of adsorption.[14,15] Coordinatively unsaturated metal sites are another strategy for enhancing CO_2 capture that has been studied and has resulted in excellent selectivities and CO_2 uptakes.[12,13] A limitation of this strategy is

Table 2. Comparison of IAST-Calculated Adsorption Capacity and Selectivity for 15/85 wt% CO_2/N_2 Mixture in Different Porous Materials

material	CO_2 loading (mmol/g)[b]	N_2 loading (mmol/g)[b]	S_{ads}[c]	initial enthalpy of adsorption, Q_s(kJ/mol)	reference
[Cu(**bcppm**)H_2O]	1.04[a]	0.010[a]	590[a]	29	this work
MgMOF-74	6.20	0.193	182[b]	39−47	12a,c,e
NaX zeolite	2.72	0.106	146[b]	31−37	36
mmen-CuBTTri	2.22	0.038	329[b]	96	15a
PPN-6-CH_2DETA	3.04	0.039	442[b]	52	14f
UTSA-16	2.37	0.043	315[b]	33	17c
SIFSIX-3-Zn			1818[d]	45	17a

[a]Data collected at 293 K. [b]296 K and 1 atm. From ref 17c. [c]15/85 wt% mixture at 296 K and 1 atm. [d]10/90 wt% mixture at 298 K and 1 atm.

dx.doi.org/10.1021/ja4032049 | J. Am. Chem. Soc. 2013, 135, 10441−10448

that other polar molecules, such as H_2O, can competitively bind to these sites and potentially mitigate their influence.[37] Further, "soft" porous materials that display gated adsorption behavior with increased CO_2 pressures have also been investigated,[7] but additional studies are required to assess the capacity of these materials to separate CO_2 in mixed gas streams.

Recent work has examined the mechanism of CO_2 capture in MOFs where limiting the degrees of freedom in a flexible structure has led to increased selectivity for CO_2 by restricting the limiting pore size of the MOF to the ultra-microporous region.[17,18,32] Due to the larger kinetic diameter of N_2 with respect to CO_2, excellent selectivity can be achieved at relatively moderate adsorption enthalpies. Zhou and co-workers described a MOF material with a dynamic structure that acts as a single-molecule trap for CO_2.[18] Similarly, investigations reticulating the chemistry of SIFSIX materials has discovered a framework displaying unprecedented levels of selectivity for CO_2 over N_2.[17a] In this present work we have used post-synthesis processing of a 2D layered material with a dynamic framework to generate a rigid, contracted framework with constricted pores possessing diameters of 3.6 Å. Controlled heating facilitates a rearrangement of the coordination sphere and changes in framework connectivity to allow a constricted pore environment to be generated. While in [Cu(**bcppm**)H_2O] the capacity is somewhat lower than that of some benchmark materials, the capacity is dictated by the need to maintain limiting pore dimensions and is in keeping with other high-performing MOF materials that utilize this approach.[17,18] Thus, the principle of pore size constriction through a post-processing mechanism demonstrates the potential to provide MOF materials with desirable characteristics for CO_2 capture.

CONCLUSION

Here we have reported the synthesis of [Cu(**bcppm**)H_2O]·*x*S from a link capable of restricted structural flexibility and copper(II) nitrate. The ceramic-like post-synthesis processing that leads to the exceptional selectivity of CO_2 over N_2 for [Cu(**bcppm**)H_2O] originates from a trellis-like movement of the 2D structure and a 2D-to-3D transformation which results in an activated material with a rigid, "locked" conformation. The rigid activated form of [Cu(**bcppm**)H_2O] has a limiting pore size of 3.6 Å that is perfectly suited for CO_2/N_2 separations and results in an IAST selectivity that places this compound in the top echelon of materials for carbon capture. Due to a low enthalpy of adsorption for CO_2, the material is also likely to have a notably low energy penalty for regeneration. Our current investigations are centered on further tuning the structure metrics of this material and exploiting this link design in the synthesis of other MOF materials that display dynamic structural changes on post-processing. The outstanding features of [Cu(**bcppm**)H_2O] have led us to commence investigations regarding the inclusion of this material into mixed-matrix membranes.

ASSOCIATED CONTENT

Supporting Information

TGA, IR spectra, further details of the PXRD experiments, gas adsorption data, details of the IAST calculations for [Cu(**bcppm**)H_2O], and single-crystal data for [Cu(**bcppm**)H_2O]-*pdes*. This material is available free of charge via the Internet at http://pubs.acs.org

AUTHOR INFORMATION

Corresponding Author

christian.doonan@adelaide.edu.au; christopher.sumby@adelaide.edu.au

Notes

The authors declare no competing financial interest.

ACKNOWLEDGMENTS

C.J.S. and C.J.D. gratefully acknowledge the Australian Research Council for funding (FT0991910 and FT100100400). This research was supported by the Science and Industry Endowment Fund. Aspects of this research were undertaken on the Powder Diffraction beamline at the Australian Synchrotron, Victoria, Australia.

REFERENCES

(1) (a) Suh, M. P.; Park, H. J.; Prasad, T. K.; Lim, D.-W. *Chem. Rev.* **2012**, *112*, 782−835. (b) Murray, L. J.; Dincâ, M.; Long, J. R. *Chem. Soc. Rev.* **2009**, *38*, 1294−1314.

(2) Li, J.-R.; Sculley, J.; Zhou, H.-C. *Chem. Rev.* **2012**, *112*, 869−932.

(3) (a) Li, J.-R.; Kuppler, R. J.; Zhou, H.-C. *Chem. Soc. Rev.* **2009**, *38*, 1477−1504. (b) D'Alessandro, D. M.; Smit, B.; Long, J. R. *Angew. Chem., Int. Ed.* **2010**, *49*, 6058−6082. (c) Li, J.-R.; Ma, Y.; McCarthy, M. C.; Sculley, J.; Yu, J.; Jeong, H.-K.; Balbuena, P. B.; Zhou, H.-C. *Coord. Chem. Rev.* **2011**, *255*, 1791−1823. (d) Sumida, K.; Rogow, D. L.; Mason, J. A.; McDonald, T. M.; Bloch, E. D.; Herm, Z. R.; Bae, T.-H.; Long, J. R. *Chem. Rev.* **2012**, *112*, 724−781.

(4) (a) Corma, A.; Garcia, H.; Llabres, F. X.; Xamena, I. *Chem. Rev.* **2010**, *110*, 4606−4655. (b) Czaja, A. U.; Trukhan, N.; Müller, U. *Chem. Soc. Rev.* **2009**, *38*, 1284−1293. (c) Lee, J.; Farha, O. K.; Roberts, J.; Scheidt, K. A.; Nguyen, S. T.; Hupp, J. T. *Chem. Soc. Rev.* **2009**, *38*, 1450−1459.

(5) (a) Eddaoudi, M.; Moler, D. B.; Li, H.; Chen, B.; Reineke, T. M.; O'Keeffe, M.; Yaghi, O. M. *Acc. Chem. Res.* **2001**, *34*, 319−330. (b) Yaghi, O. M.; O'Keeffe, M.; Ockwig, N. W.; Chae, H. K.; Eddaoudi, M.; Kim, J. *Nature* **2003**, *423*, 705−714. (c) Férey, G. *Chem. Soc. Rev.* **2008**, *37*, 191−214. (d) Zhou, H.-C.; Long, J. R.; Yaghi, O. M. *Chem. Rev.* **2012**, *112*, 673−674. (e) Cook, T. R.; Zheng, Y.-R.; Stang, P. J. *Chem. Rev.* **2013**, *113*, 734−777.

(6) (a) Kitagawa, S.; Kitaura, R.; Noro, S. *Angew. Chem., Int. Ed.* **2004**, *43*, 2334−2375. (b) Kitagawa, S.; Uemura, K. *J. Solid State Chem.* **2005**, *178*, 2420−2429.

(7) (a) Suh, M. P.; Cheon, Y. E.; Lee, E. Y. *Coord. Chem. Rev.* **2008**, *252*, 1007−1026. (b) Horike, S.; Shimomura, S.; Kitagawa, S. *Nat. Chem.* **2009**, *1*, 695−704. (c) Férey, G.; Serre, C. *Chem. Soc. Rev.* **2009**, *38*, 1380−1399. (d) Keene, T. D.; Rankine, D.; Evans, J. D.; Southon, P. D.; Kepert, C. J.; Aitken, J. B.; Sumby, C. J.; Doonan, C. J. *Dalton Trans.* **2013**, *42*, 7871−7879. (e) Lyndon, R.; Konstas, K.; Ladewig, B. P.; Southon, P. D.; Kepert, P. C. J.; Hill, M. R. *Angew. Chem., Int. Ed.* **2013**, *52*, 3695−3698. (f) Bloch, W. M.; Sumby, C. J. *Chem. Commun.* **2012**, *48*, 2534−2536.

(8) (a) Jia, Q. X.; Wang, Y.-Q.; Yue, Q.; Wang, Q.-L.; Gao, E.-Q. *Chem. Commun.* **2008**, 4894−4896. (b) Kitagawa, S.; Uemura, K. *Chem. Soc. Rev.* **2005**, *34*, 109−119. (c) Serre, C.; Mellot-Draznieks, C.; Surblé, S.; Audebrand, N.; Filinchuk, Y.; Férey, G. *Science* **2007**, *315*, 1828−1831. (d) Maji, T. K.; Uemura, K.; Chang, H.-C.; Matsuda, R.; Kitagawa, S. *Angew. Chem., Int. Ed.* **2004**, *43*, 3269−3272.

(9) (a) Uemura, K.; Kitagawa, S.; Fukui, K.; Saito, K. *J. Am. Chem. Soc.* **2004**, *126*, 3817−3828. (b) Uemura, K.; Kitagawa, S.; Kondo, M.; Fukui, K.; Kitaura, R.; Chang, H.-C.; Mizutani, T. *Chem.—Eur. J.* **2002**, *8*, 3586−3600.

(10) (a) Biradha, K.; Fujita, M. *Angew. Chem., Int. Ed.* **2002**, *41*, 3392−3395. (b) Lim, K. S.; Ryu, D. W.; Lee, W. R.; Koh, E. K.; Kim, H. C.; Hong, C. S. *Chem.—Eur. J.* **2012**, *18*, 11541−11544. (c) Biradha, K.; Hongo, Y.; Fujita, M. *Angew. Chem., Int. Ed.* **2002**, *41*, 3395−3398. (d) Nakagawa, K.; Tanaka, D.; Horike, S.;

Shimomura, S.; Higuchi, M.; Kitagawa, S. *Chem. Commun.* **2010**, *46*, 4258−4260.
(11) Ferey, G.; Serre, C. *Chem. Soc. Rev.* **2009**, *38*, 1380−1399.
(12) For examples, see: (a) Britt, D.; Furukawa, H.; Wang, B.; Glover, T. G.; Yaghi, O. M. *Proc. Natl. Acad. Sci. U.S.A.* **2009**, *106*, 20637−20640. (b) Mason, J. A.; Sumida, K.; Herm, Z. R.; Krishna, R.; Long, J. R. *Energy Environ. Sci.* **2011**, *4*, 3030−3040. (c) Dietzel, P. D. C.; Besikiotis, V.; Blom, R. *J. Mater. Chem.* **2009**, *19*, 7362−7370. (d) Zhou, W.; Wu, H.; Yildirim, T. *J. Am. Chem. Soc.* **2008**, *130*, 15268−15269. (e) Caskey, S. R.; Wong-Foy, A. G.; Matzger, A. J. *J. Am. Chem. Soc.* **2008**, *130*, 10870−10871.
(13) (a) Bae, Y.-S.; Hauser, B. G.; Farha, O. K.; Hupp, J. T.; Snurr, R. Q. *Microporous Mesoporous Mater.* **2011**, *141*, 231−235. (b) Fang, Q. R.; Zhu, G. S.; Xue, M.; Sun, J. Y.; Wei, Y.; Qiu, S. L.; Xu, R. R. *Angew. Chem., Int. Ed.* **2005**, *44*, 3845−3848. (c) Bloch, E. D.; Britt, D.; Lee, C.; Doonan, C. J.; Uribe-Romo, F. J.; Furukawa, H.; Long, J. R.; Yaghi, O. M. *J. Am. Chem. Soc.* **2010**, *132*, 14382−14384.
(14) For examples, see: (a) An, J.; Geib, S. J.; Rosi, N. L. *J. Am. Chem. Soc.* **2009**, *132*, 38−39. (b) McDonald, T. M.; Lee, W. R.; Mason, J. A.; Wiers, B. M.; Hong, C. S.; Long, J. R. *J. Am. Chem. Soc.* **2012**, *134*, 7056−7065. (c) Liao, P.-Q.; Zhou, D.-D.; Zhu, A.-X.; Jiang, L.; Lin, R.-B.; Zhang, J.-P.; Chen, X.-M. *J. Am. Chem. Soc.* **2012**, *134*, 17380−17383. (d) Yang, E.; Li, H.-Y.; Wang, F.; Yang, H.; Zhang, J. *CrystEngComm* **2013**, *15*, 658−661. (e) Burd, S. D.; Ma, S.; Perman, J. A.; Sikora, B. J.; Snurr, R. Q.; Thallapally, P. K.; Tian, J.; Wojtas, L.; Zaworotko, M. J. *J. Am. Chem. Soc.* **2012**, *134*, 3663−3666. (f) Lu, W.; Sculley, J. P.; Yuan, D.; Krishna, R.; Wei, Z.; Zhou, H.-C. *Angew. Chem., Int. Ed.* **2012**, *51*, 7480−7484.
(15) (a) McDonald, T. M.; D'Alessandro, D. M.; Krishna, R.; Long, J. R. *Chem. Sci.* **2011**, *2*, 2022−2028. (b) Demessence, A.; D'Alessandro, D. M.; Foo, M. L.; Long, J. R. *J. Am. Chem. Soc.* **2009**, *131*, 8784−8786. (c) Gu, J.-M.; Kwon, T.-H.; Park, J.-H.; Huh, S. *Dalton Trans.* **2010**, *39*, 5608−5610.
(16) (a) Mason, J. A.; Sumida, K.; Herm, Z. R.; Krishna, R.; Long, J. R. *Energy Environ. Sci.* **2011**, *4*, 3030−3040. (b) Wiersum, A. D.; Chang, J.-S.; Serre, C.; Llewellyn, P. L. *Langmuir* **2013**, *29*, 3301−3309.
(17) (a) Nugent, P.; Belmabkhout, Y.; Burd, S. D.; Cairns, A. J.; Luebke, R.; Forrest, K.; Pham, T.; Ma, S.; Space, B.; Wojtas, L.; Eddaoudi, M.; Zaworotko, M. J. *Nature* **2013**, *495*, 80−84. (b) Li, J.-R.; Yu, J.; Lu, W.; Sun, L.-B.; Sculley, J.; Balbuena, P. B.; Zhou, H.-C. *Nat. Commun.* **2013**, *4*, No. 1538. (c) Xiang, S.; He, Y.; Zhang, Z.; Wu, H.; Zhou, W.; Krishna, R.; Chen, B. *Nat. Commun.* **2012**, *3*, No. 954. (d) Lau, C. H.; Babarao, R.; Hill, M. R. *Chem. Commun.* **2013**, *49*, 3634−3636.
(18) Wriedt, M.; Sculley, J. P.; Yakovenko, A. A.; Ma, Y.; Halder, G. J.; Balbuena, P. B.; Zhou, H.-C. *Angew. Chem., Int. Ed.* **2012**, *51*, 1−6.
(19) For examples, see: (a) Choi, H. S.; Suh, M. P. *Angew. Chem., Int. Ed.* **2009**, *48*, 6865−6869. (b) Henke, S.; Schneemann, A.; Wutscher, A.; Fischer, R. A. *J. Am. Chem. Soc.* **2012**, *134*, 9464−9474. (c) Seo, J.; Matsuda, R.; Sakamoto, H.; Bonneau, C.; Kitagawa, S. *J. Am. Chem. Soc.* **2009**, *131*, 12792−12800. (d) Zhang, J.; Wu, H.; Emge, T. J.; Li, J. *Chem. Commun.* **2010**, *46*, 9152−9154. (e) Kim, T. K.; Suh, M. P. *Chem. Commun.* **2011**, *47*, 4258−4260. (f) Hong, D. H.; Suh, M. P. *Chem. Commun.* **2012**, *48*, 9168−9170.
(20) Robeson, L. M. *J. Membr. Sci.* **1991**, *62*, 165−185.
(21) (a) Potapov, A. S.; Khlebnikov, A. I. *Polyhedron* **2006**, *25*, 2683−2690. (b) Potapov, A. S.; Khlebnikov, A. I.; Valisevskii, S. F. *Russ. J. Org. Chem.* **2006**, *42*, 1368−1373.
(22) Sheldrick, G. M. *Acta Crystallogr.* **1990**, *A46*, 467−473.
(23) Sheldrick, G. M. *SHELXL-97*; University of Göttingen: Göttingen, Germany, 1997.
(24) Barbour, L. J. *J. Supramol. Chem.* **2001**, *1*, 189−191.
(25) *CrystalMaker 2.3.2*; CrystalMaker Software Ltd.: Oxfordshire, UK, 2011.
(26) Sheldrick, G. M. *CIFTAB*; University of Göttingen: Göttingen, Germany, 1997.
(27) Spek, A. L. *Acta Crystallogr.* **1990**, *A46*, C34.
(28) *Mercury 2.4*; Cambridge Crystallographic Data Centre: Cambridge, UK, 2010.
(29) Gelb, L. D.; Gubbins, K. E. *Langmuir* **1999**, *15*, 305−308.
(30) (a) Rappe, A. K.; Casewit, C. J.; Colwell, K. S.; Goddard, W. A.; Skiff, W. M. *J. Am. Chem. Soc.* **1992**, *114*, 10024−10035. (b) Hirotani, A.; Mizukami, K.; Miura, R.; Takaba, H.; Miya, T.; Fahmi, A.; Stirling, A.; Kubo, M.; Miyamoto, A. *Appl. Surf. Sci.* **1997**, *120*, 81−84.
(31) Myers, A. L.; Prausnitz, J. M. *AIChE J.* **1965**, *11*, 121−127.
(32) Bae, Y.-S.; Farha, O. K.; Hupp, J. T.; Snurr, R. Q. *J Mater. Chem.* **2009**, *19*, 2131−2134.
(33) Kole, G. K.; Vittal, J. J. *Chem. Soc. Rev.* **2013**, *42*, 1755−1775.
(34) Moon, J.-H.; Bae, Y.-S.; Hyun, S.-H.; Lee, C.-H. *J. Membr. Sci.* **2006**, *285*, 343−359.
(35) Jagiello, J.; Thommes, M. *Carbon* **2004**, *42*, 1227−1232.
(36) (a) Belmabkhout, Y.; Pirngruber, G.; Jolimaitre, E.; Methivier, A. *Adsorption* **2007**, *13*, 341−349. (b) Cavenati, S.; Grande, C. A.; Rodrigues, A. E. *J. Chem. Eng. Data* **2004**, *49*, 1095−1101.
(37) Kizzie, A. C.; WongFoy, A. G.; Matzger, A. J. *Langmuir* **2011**, *27*, 6368−6367.